Lateral Acceleration Control Design of a Non-Linear Homing Missile using Multi-Objective Evolution Strategies

T. Sreenuch, A. Tsourdos, E. J. Hughes, and B. A. White

Department of Aerospace, Power & Sensors

Cranfield University (RMCS Shrivenham)

Swindon SN6 8LA, ENGLAND

Abstract— **The paper presents the lateral acceleration control design of non-linear missile model using the multiple single objective Pareto sampling method. The interpolated controller design for the uncertain plants is carried out by minimizing gain and phase margins, tracking and actuator rate limit frequency domain based performance objectives. An ad-hoc approach is taken to the controller interpolation. The controller's trade-offs are analyzed using the obtained Pareto optimal solutions (corresponding to a given set of weight vectors). The non-linear simulation results show that the selected interpolated controller is a robust tracking controller for all perturbation vertices.**

I. INTRODUCTION

This paper looks at the application of multi-objective evolutionary optimization to a robust autopilot design. The aim is to synthesize the fixed-structure controller by shaping the system's open and closed-loop frequency responses results in the closed-loop responses are within the tracking bounds. However, the demanded fast closed-loop responses are constrained by the fin's rate limit. In this work, the actuator sluggishness is avoided by limiting the demanded fin angle response at high frequency to be within the maximum fin deflection rate for a step input. Finding a feasible control structure (and furthermore tuning it) that meet the frequency bounds can be very difficult, and the resulting interpolated controller may not be stabilizing. By formulating the former to an optimization problem, the specific solutions on the Pareto front can be identified using the evolution strategy (ES) and target vector method. Note that the ES allows the inner and outer loop-shaping to be carried out simultaneously. The resulting linear controllers are interpolated using a soundly-based gain scheduling approach.

This paper is organized as follows: The missile's lateral dynamics and autopilot requirements are described in section II. The problem formulation, the stability constraints and frequency domain based objective functions, is stated in section III. The implication of trade-offs and simulation results are presented in section IV.

II. MISSILE MODEL AND AUTOPILOT REQUIREMENTS

A. Non-Linear Model

The missile model used in this study is taken from Horton's MSc thesis [1]. It describes a 5 DOF model in parametric format with severe cross-coupling and non-linear behavior. This study will look at the reduced problem of a 2 DOF controller for the lateral motion (on the xy plane in Fig. 1). The airframe is roll stabilized ($\lambda = 45°$), and no
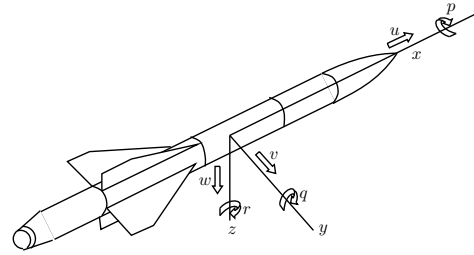

Fig. 1.   Airframe axes and nomenclature.

coupling is assumed between pitch and yaw channels. With these assumptions, the equations of motion are given by

$$\dot{v} = y_v(M,\sigma)v + y_\zeta(M,\sigma)\zeta - Ur,$$
$$= \frac{1}{2m}\rho VS(C_{y_v}v + VC_{y_\zeta}\zeta) - Ur,$$
$$\dot{r} = n_v(M,\sigma)v + n_r(M,\sigma)r + n_\zeta(M,\sigma)\zeta,$$
$$= \frac{1}{2I_z}\rho VSd(C_{n_v}v + \frac{1}{2}dC_{n_r}r + VC_{n_\zeta}\zeta) \quad (1)$$

where the variables are defined in Fig. 1. Here v is the side-slip velocity, r is the body rate, ζ is the rudder fin deflections, y_v, y_ζ are semi-non-dimensional force derivatives due to lateral velocity and fin angle, n_v, n_r, n_ζ are semi-non-dimensional force derivatives due to side-slip velocity, body rate and fin angle. U is the forward velocity. Furthermore, $m = 150$ kg (125 kg) is the missile mass when full (all burnt), $\rho = \rho_0 - 0.094h$ is the air density ($\rho_0 = 1.23$ kg/m^3 is the sea level air density and h is the missile altitude in km), V is the total velocity in m/s, $S = \pi d^2/4 = 0.0314$ m^2 is the reference area ($d = 0.2$ m is the reference diameter) and $I_z = 75$ kg·m^2 (60 kg·m^2) is the lateral inertia when full (all burnt). For the coefficients C_{y_v}, C_{y_ζ}, C_{n_v}, C_{n_r}, C_{n_ζ} only discrete data points are available, obtained from wind tunnel experiments. The interpolation formulas, involving the Mach number M and incidence σ, have been evaluated with the results summarized in Table I. $V = \sqrt{U^2 + v^2}$ is to total velocity. It is assumed that $U \gg v$, so that the total incidence σ can thus be taken as $\sigma = v/U$, as $\sin\sigma \approx \sigma$ for small σ. Finally, the Mach number is obviously defined as $M = V/a$, where $a = 340$ m/s is the speed of sound.

Aerodynamic derivative	Interpolated formula
C_{y_v}	$-26 + 1.5M - 60|\sigma|$
C_{y_ζ}	$-10 + 1.4M - 1.5|\sigma|$
C_{n_r}	$-500 - 30M + 200|\sigma|$
C_{n_v}	$s_m C_{y_v}$, where $s_m = d^{-1}[(1.3 + m/500) \\ \qquad -(1.3 + 0.1M + 0.3|\sigma|)]$
C_{n_ζ}	$s_f C_{y_\zeta}$, where $s_f = d^{-1}[(1.3 + m/500) - 2.6]$

TABLE I

AERODYNAMIC DERIVATIVES OF THE NON-LINEAR MODEL.

Fig. 3.   Velocity operating envelope.

B. 2 DOF Autopilot Configuration

The lateral autopilot configuration used in this paper is shown in Fig. 2, where $F(s) = 98700/(s^2 + 445s + 98700)$
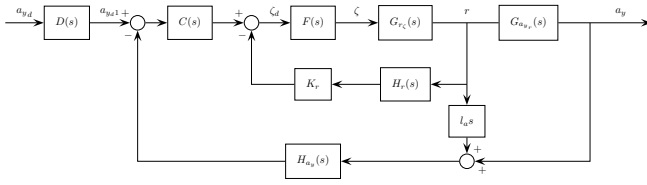

Fig. 2.   2 DOF autopilot configuration.

is the fin servo dynamics with maximum fin angle of ± 0.3 rad and rate of ± 15 rad/s, $H_r(s) = 253000/(s^2 + 710s + 253000)$ is the rate gyro dynamics, $H_{a_y}(s) = 394800/(s^2 + 890s + 394800)$ is the lateral accelerometer dynamics and $l_a = 0.9$ m (0.8 m) is the accelerometer moment arm when full (all burnt). The open-loop transmission

$$G_{r_\zeta}(s) = \frac{n_\zeta s - (n_\zeta y_v - n_v y_\zeta)}{s^2 - (y_v + n_r)s + (Un_v + y_v n_r)} \quad \text{and}$$

$$G_{a_{y_r}}(s) = \frac{y_\zeta s^2 - y_\zeta n_r s - U(n_\zeta y_v - n_v y_\zeta)}{n_\zeta s - (n_\zeta y_v - n_v y_\zeta)} \quad (2)$$

represent the missile dynamics, obtained by linearizing (1).

C. Closed-Loop Performance Specifications

The autopilot is required to track a lateral acceleration demand a_{y_d} over the whole flight envelope (see Fig. 3). The airframe is constrained by limitations on structure integrity, and for a modern missile requiring high maneuverability a typical maximum lateral acceleration $a_{y_{max}}$ will be ± 500 m/s^2. Recall that $\sigma = v/U$, σ_{max} can thus be found by equating (1) to $\vec{0}$ and using the relationship $a_{y_{ss}} = Ur_{ss}$. The operating envelope of the Mach number M and incidence σ corresponding to $a_{y_{max}} = \pm 500$ m/s^2 is calculated and shown in figure 4.

Moreover, the autopilot must also be as robust to the variation in mass m (the propellant is constantly burned) and uncertainty in aerodynamic derivatives $(\Delta_{C_{y_v}}, \Delta_{C_{y_\zeta}}, \Delta_{C_{n_v}}, \Delta_{C_{n_r}}, \Delta_{C_{n_\zeta}} = \pm 5\%)$, and not being upset by fin saturation and sluggishness.
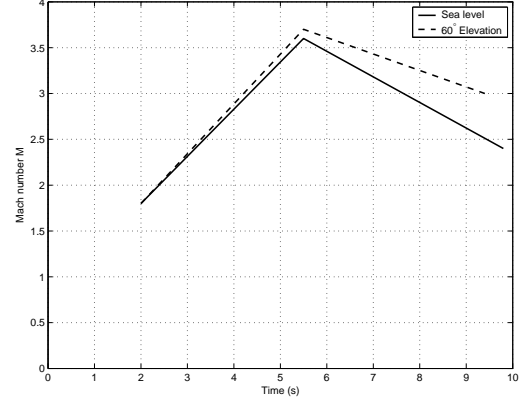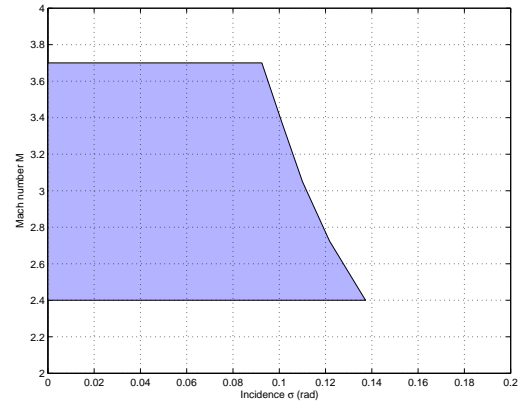

Fig. 4.   Operating envelope.

A list of performance specification (for a unit-step input) is given in the time-domain using familiar figures as follows:

1. Settling time $t_s < 0.25$ s,
2. Settling time variation $|\delta_{t_s}| \le 0.05$ s,
3. Steady state error $e_{ss} \le 10$ %,
4. Damping ratio $\zeta_{a_y} \approx 0.7$,
5. Gain margin $GM \ge 9$ dB, Phase margin $PM \ge 40°$.
6. Fin deflection $|\zeta| \le 0.0006$ rad, fin deflection rate $|\dot{\zeta}| \le 0.015$ rad/s.

From the results obtained in Fig. 4, the required fin angle ζ_{ss} is well within the saturation level. Hence, the actuator saturation problem can be safely ignored in this case.

III. DESIGN OF LATERAL MISSILE AUTOPILOT

A. Internal Stability

The sufficient and necessary condition for the robust stability of the closed-loop systems (depicted in Figure 2) is that

1. $T(s) = a_y(s)/a_{y_d}(s)$ is stable.
2. A non-minimum phase zero of $G_{a_{y_\zeta}}(s)$ is not canceled by an unstable pole of $C(s)$.

In this work, the stability of $T(s)$ is determined by solving the roots of the characteristic polynomial. To ensure internal

stability, a minimum and stable $C(s)$ is desired. This can guarantee no RHP pole (and zero) cancellations.

B. Frequency Domain Performance Requirements

In this paper, the tracking performance specifications are modeled in the frequency domain requirements which have a convenient graphical interpretation in terms of tracking ratios. With the design objectives given in section II-C, the controller's performances can then be measured by evaluating the following robustness assessment functions:

1) Gain and Phase Margins Based Cost Function: A look at the Nichols Chart qualitatively reveals that gain and phase margin can be defined in term of $\max_{\omega} |T(j\omega)|$, where $T(s)$ is for now defined as a unity-feedback closed-loop transmission ratio [2]. For instance, if $|T(j\omega)| \leq M_p = 3$ dB, then $GM > 4$ dB and $PM > 45°$ are guaranteed (see Figure 5).
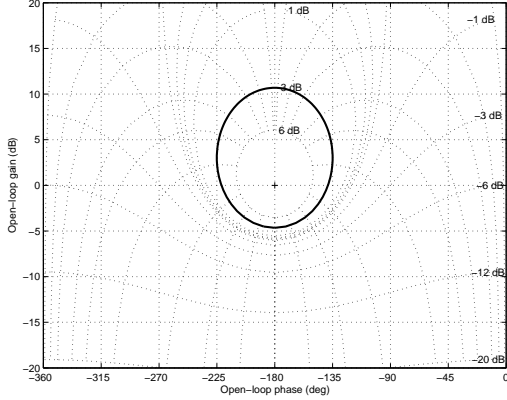

Fig. 5.   Nichols chart.

Adopting these relationships, the gain and phase margin based cost function can be given by

$$J_{2_{ij}} = \begin{cases} \displaystyle \max_{\omega_{L_1} \leq \omega \leq \omega_{U_1}} \frac{|T_{1_{ij}}(j\omega)| - M_0}{M_{p_1} - M_0} & \text{if } T_{1_{ij}}(s) \text{ is stable,} \\ \Omega & \text{otherwise,} \end{cases}$$

(3)

where $T_1(s) = a_y(s)/a_{yd1}(s)$, j is the operating region Q_i's vertices index, M_{p_1} is the peak magnitude constraint, M_0 is -6 dB constant gain contour, and Ω is some large number.

By using a standard block diagram reduction rules, $L(s)$ can be written as

$$L(s) = \frac{-C(s)F(s)(l_a s G_{r_\zeta}(s) + G_{a_{y_\zeta}}(s))H_{a_y}(s)}{1 - K_r F(s) G_{r_\zeta}(s) H_r(s)}.$$

(4)

But then $|l_a j\omega G_{r_\zeta}(j\omega) + G_{a_{y_\zeta}}(j\omega)| \leq |G_{a_{y_\zeta}}(j\omega)|$ and $\angle -(l_a(j\omega)G_{r_\zeta}(j\omega) + G_{a_{y_\zeta}}(j\omega)) \geq \angle -G_{a_{y_\zeta}}(j\omega)$ (see Fig. 6), thus the achieved gain and phase margins will always be greater than or equal to the designed values.
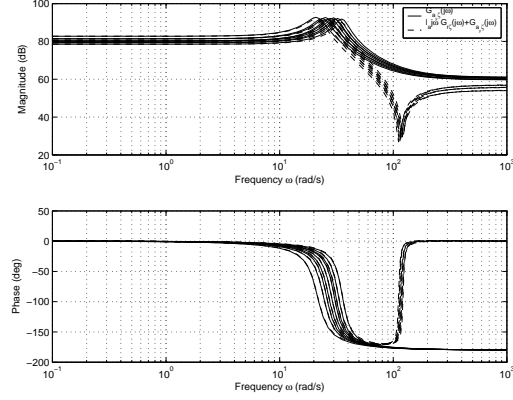

Fig. 6.   Frequency responses of the Q_i's nominal $-G_{a_{y_\zeta}}(s)$ and $-(l_a s G_{r_\zeta}(s) + G_{a_{y_\zeta}}(s))$.
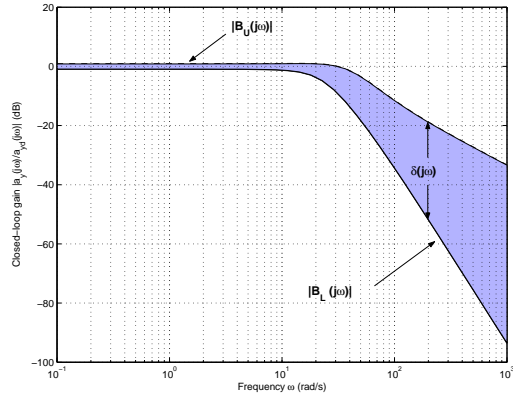

Fig. 7.   Frequency domain response specifications.

2) Tracking Boundaries Based Cost Function: The system's tracking performance specifications are based upon satisfying all of the frequency forcing functions $|B_U(j\omega)|$ and $|B_L(j\omega)|$ shown in Fig. 7. They represent the upper and lower bounds of tracking performance specifications whom an acceptable response $|T(j\omega)|$ must lie within [3].

Following this design concept, the tracking boundaries based cost function can be defined by,

$$J_{3_{ij}} = \max_{\omega_L \leq \omega \leq \omega_U} \left\{ \frac{|T_{ij}(j\omega)| - |T_0(j\omega)|}{|B_U(j\omega)| - |T_0(j\omega)|}, \frac{|T_0(j\omega)| - |T_{ij}(j\omega)|}{|T_0(j\omega)| - |B_L(j\omega)|} \right\},$$

(5)

where $T_0(j\omega)$ is the nominal tracking ratio. Note that ω_U is defined to be the frequency at which $|T_0(j\omega)| = -12$ dB. This frequency range is considered to be sufficient for the resulting time response approximation.

3) Actuator Rate Limit Based Cost Function: The fin servo can be modeled as a linear dynamic part $F(s)$ and a series rate limiter illustrated in Figure 8. The input to the integrator cannot exceed the limit R, i.e. the output of the rate limiter $\zeta_{d_{lim}}$ satisfies $|\dot\zeta_{d_{lim}}| \leq R$. Now consider a sinusoidal input

$$\zeta_d = A \sin \omega t.$$

(6)

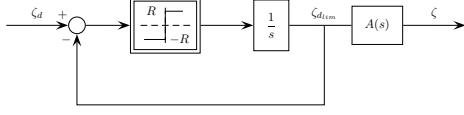Fig. 8. Actuator with rate limiter and linear dynamics $F(s)$.

$\zeta_{d_{lim}}$'s steady-state response is in the linear range (i.e. $\zeta_{d_{lim}}(t) = \zeta_d(t) = A\sin\omega t$) if $A\omega \leq R$. Thus, the rate saturation can be avoided by limiting the demanded fin angle ($T_2(s) = \zeta_d(s)/a_{y_d}(s)$) gain-bandwidth product to be R, where R is from now the maximum fin deflection rate for a unit-step input.

Using these results, the actuator rate limit based cost function can be given by

$$J_{4_{ij}} = \max_{\omega_{L_2} \leq \omega \leq \omega_{U_2}} \frac{|T_{2_{ij}}(j\omega)|\omega}{R}. \tag{7}$$

IV. Optimization

A. Multi-Objective Evolutionary Optimization Algorithms

Basic scheme of the multi-objective evolution strategy $((\mu + \lambda)$-ES) used in this paper is as that described in. Instead of, using non-dominated ranking, finding all Pareto solutions, it locates some specific solutions on the Pareto front corresponding to a given set of target vectors (e.g. weighted Min-Max) $V = \{\vec{v}_1, \ldots, \vec{v}_T\}$ [4]. Each generation, T weighted Min-Max distances are evaluated for all $\mu + \lambda$ solutions, whose results are held in a matrix $S = (s_{ij})$. Note that

$$s_{ij} = \max_{j=1,\ldots,4} w_j^{(k)} O_i^{(k)}, \tag{8}$$

where $w_j^{(k)} = 1/v_j^{(k)}$ and $O_i^{(k)}$ is ith individual's kth objective value. Each column of the matrix S is then ranked, with the best score population member on the corresponding target vector being given a rank of 1, and the worst a rank of $\mu + \lambda$. The rank values are stored in a matrix R. Now R can be used to rank the population based on the number of target vectors that are satisfied the best.

The primary advantages of this method is such that the target vectors can be arbitrary generated focusing on the interested regions. Also the limits of the objective space and discontinuities within the Pareto set can be identified by observing the distribution of the angular errors ($\theta_i = \cos^{-1}\hat{v}_j \cdot \hat{O}_i$) across the total weight set.

B. Robust Gain-Scheduled Controller

1) Feasible Fixed-Structure Controller: Suppose the controller's order is prespecified (e.g. K_r, $C(s) = K_p(s + z_p)/(s + p_p)$ and $D(s) = K_f(s + z_f)/(s + p_f)$). Then, the optimization variables are K_r, K_p, z_p, p_p, K_d, z_d and p_d. This is similar for difference control structures. Likewise classical loop-shaping, these set of parameters are then translated into the logarithmic space, thus

$$\vec{x} = [\bar{K}_r, \bar{K}_p, \bar{z}_p, \bar{p}_p, \bar{K}_d, \bar{z}_d, \bar{p}_d], \tag{9}$$

where $\bar{K}_r = \log_{10} K_r$, $\bar{K}_p = \log_{10} K_p$, etc..., is now formed a variables vector for the ES. This allows quite large ranges of all the parameters to be explored, and proves to speed up the convergence of the ES.

Consider the operating region $2.725 \leq M \leq 3.05$ and $0.0275 \leq \sigma \leq 0.0825$. Let $M_p = 3$ dB and demanded settling time $t_{s_d} = 0.2$ s. J_4 is for now considered as a constraint. Pursuing the method described in section IV-A , the Pareto-optimal solutions (where $0.1 \leq w^{(k)} \leq 1.0$) for difference control structures are shown in Fig. 10. It can
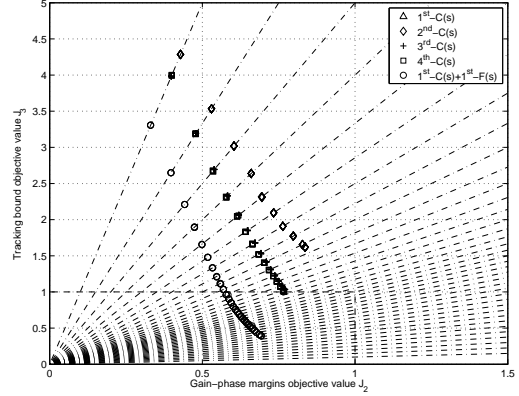

Fig. 9. Pareto-optimal solutions for difference control structures at 500th generation.

be seen that a low-order feasible controller can be achieved with an additional of a prefilter $F(s)$. This result is intuitive since in 2 DOF systems there is no direct relationship between the stability margins of the feedback system and its time-domain response.

2) Design of Linear Interpolated Controller: Using the fixed-structure controller described in section IV-*B-1*, we take an ad-hoc approach to the interpolation where the controllers are interpolated by interpolation of poles, zeros and gains [5]. Instead of using piecewise linear interpolation, the controller's poles, zeros and gains are relatively simpler formulated as linear function of Mach number M and incidence σ ($K_r = k_r^{(0)} + k_{r_M}^{(0)} + (k_r^{(1)} + k_{r_M}^{(1)} M)|\sigma|$, $K_p = k_p^{(0)} + k_{p_M}^{(0)} + (k_p^{(1)} + k_{p_M}^{(1)} M)|\sigma|$, etc...), whose coefficients ($k_r^{(0)}$, $k_{r_M}^{(0)}$,...,$p_{d_M}^{(1)}$) straightforwardly are now the optimization variables.

In addition, the operating regions are suggested to be overlapped as an attempt to preserve the stability and performance of the resulting interpolated controller (see Fig. 10). By trial and error, 9 subdivisions of the operating range is sufficient in this case.

Now recall that the small settling time t_s is required besides acceptable stability margins, tracking responses and fin rate (see section II-*C*). Thus, addition optimization variable t_{s_d} and objective function $J_1 = t_{s_d}/t_{s_{max}}$ are needed, where t_{s_d} is the demanded settling time and $t_{s_{max}} = 0.25$ s. Hence,

$$\vec{x} = [t_{s_d}, \bar{k}_r^{(0)}, \ldots, \bar{p}_{f_M}^{(1)}] \tag{10}$$
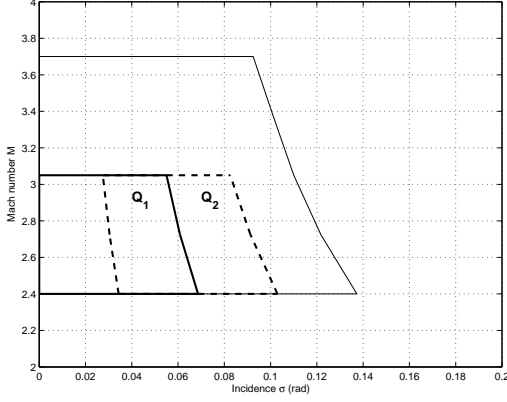
Fig. 10. Two overlap operating regions.

Fig. 12. Q_i' nominal open-loop frequency responses.

is therefore a new variables vector.

Following the initial design, the cumulative trade-off graphs (where $0.5 \leq w^{(k)} \leq 1.0$) for the linear interpolated controller is shown in Fig. 11. Note that when the
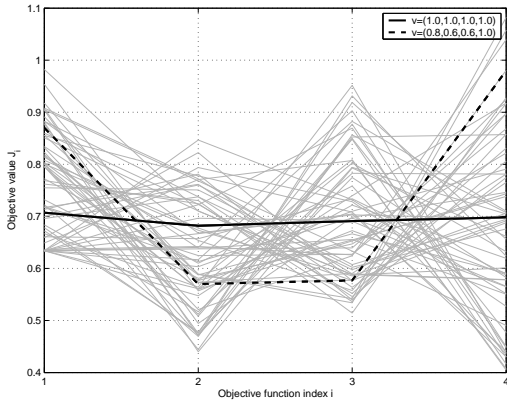

Fig. 11. Cumulative trade-off graph of the linear interpolated controller at 500th-generation.

design linear controllers are interpolated, the actual non-linear performances of the resulting controller are likely to degrade. Thus, the solution associated with the target vector $(0.8, 0.6, 0.6, 1.0)$ is preferred in this case (dashed line in Fig. 11). Its results corresponding to the minimizing objectives are in Table II and Fig.12-14. The resulting

Poles, Zeros and Gains	Interpolated formula
K_r	$0.0662 + 1.092 \times 10^{-5}M + (0.00136 - 0.00864M)|\sigma|$
K_p	$0.000256 - 1.457 \times 10^{-7}M + (2.056 \times 10^{-5} + 5.621 \times 10^{-6})|\sigma|$
z_p	$32.616 + 0.379M + (3.547 + 1.167M)|\sigma|$
p_p	$14.183 + 0.124M + (-13.024 - 0.252M)|\sigma|$
K_f	$0.0536 + 2.681 \times 10^{-5}M + (-0.00423 + 0.000295M)\sigma|$
z_f	$613.783 + 1.468M + (29.178 + 1.166M)|\sigma|$
p_f	$26.471 - 0.263M + (-1.935 - 0.164M)|\sigma|$

TABLE II

POLES, ZEROS AND GAINS INTERPOLATED FORMULAS.

design has a relative small settling time, satisfied fin rate limit, and more importantly good robustness properties (sta-
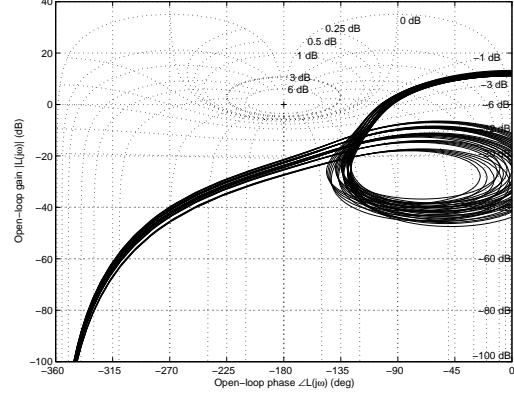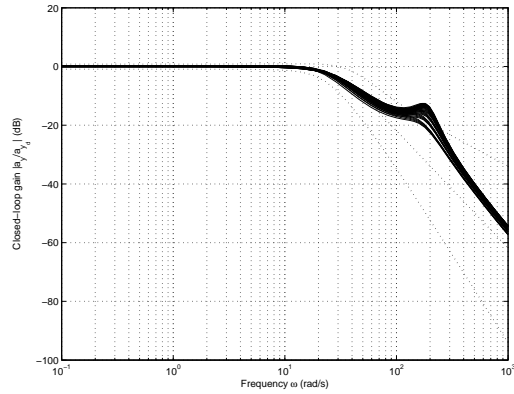

Fig. 13. Q_i' nominal closed-loop frequency responses.

bility margins and tracking performances. Notice that the influence of the non-minimum phase zero on the demanded fin angle frequency response (occurrence of the side-lope) is clearly visible (see Fig. 14). Employing the non-linear 2 DOF model described in section II-*A* (including the rate limiter), the time responses of the interpolated controller are shown in Fig 15. The simulation results show that the resulting controller is robust for all perturbation vertices.

V. CONCLUSIONS

The paper presents the lateral acceleration control design of a non-linear missile model using the multi-objective evolutionary optimization method. The aim is to arrive with a fast closed-loop response without violating the actuator constraints. In this work, this fin rate constraint function is formulated in term of the gain-frequency product. The feasible controller is initially determined by analyzing the Pareto optimal solutions (point-wise design) for difference control structures. The result shows that a low-order feasible controller can achieved with the additional of a prefilter. Using the described fixed-structure controller, the interpolated controller, whose poles, zeros and gains are linear function of Mach number M and incidence σ, is chosen from the cumulative trade-offs graph (corresponding to a given set of weight vectors). The non-linear simulation results show
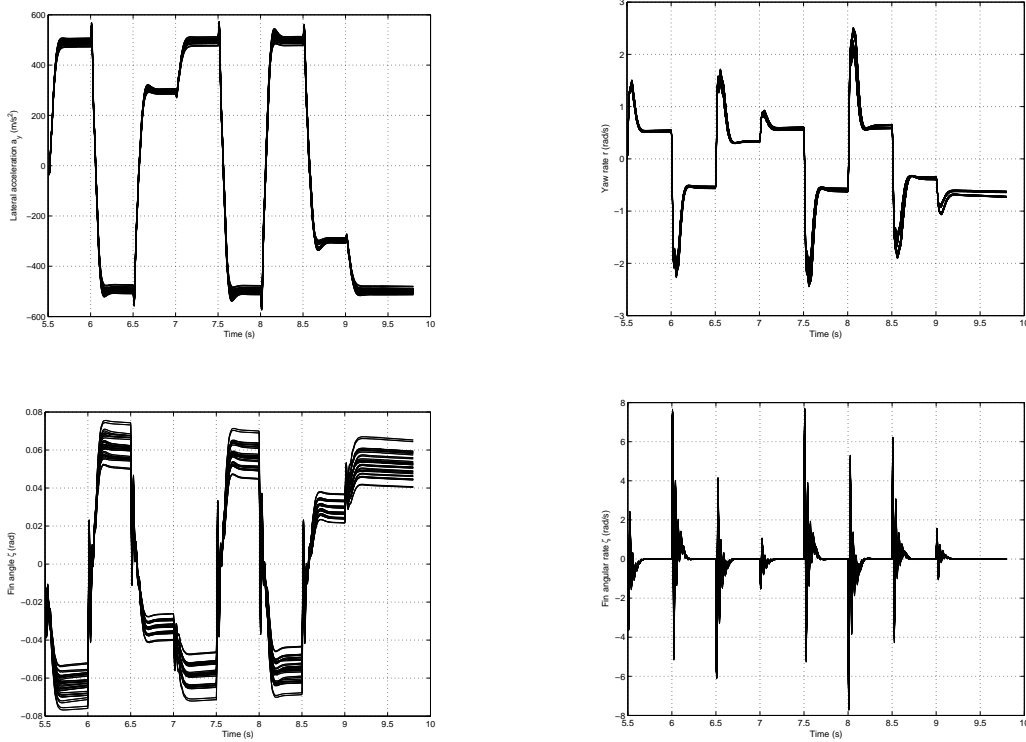
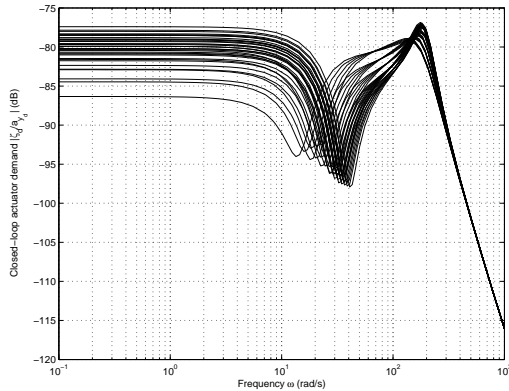Fig. 15. Lateral acceleration control responses of the perturbed systems.

Fig. 14. Q_i' nominal closed-loop actuator demand frequency responses.

that the selected interpolated controller is indeed robust for all perturbation vertices.

REFERENCES

[1] M. P. Horton. A study of autopilots for the adaptive control of tactical guided missiles. Master's thesis, University of Bath, Bath, UK, 1992.

[2] M. Sidi. *Design of Robust Control Systems: From Classical to Modern Practical Approaches*. Krieger, Malabar, Florida, 2001.

[3] C. H. Houpis and S. J. Rasmussen. *Quantitative Feedback Theory: Fundamentals and Applications*. Control Engineering. Marcel Dekker, New York, 1999.

[4] E. J. Hughes. Multiple single objective pareto sampling. In *the Congress on Evolutionary Computations*, Canberra, December 2003.

[5] R. A. Nichols, R. T. Reichert, and W. J. Rugh. Gain scheduling for $\mathcal{H}_\infty$ controllers: A flight control example. *IEEE Transactions on Control Systems Technology*, 1(2):69–79, June 1993.